Simultaneous Modulation and Fiber-Optic Transmission of 10-Gb/s Baseband and 60-GHz-Band Radio Signals on a Single Wavelength

Tomotada Kamisaka, Toshiaki Kuri, *Member, IEEE*, and Ken-ichi Kitayama, *Senior Member, IEEE*

***Abstract*—A simultaneous modulation and fiber-optic transmission of a 10-Gb/s baseband signal and a 60-GHz RF signal with 155-Mb/s differential-phase-shift-keying (DPSK) data on a single wavelength is investigated. To the authors' knowledge, it is experimentally demonstrated for the first time that both a 10-Gb/s on–off-keying baseband signal and a 60-GHz RF signal with 155-Mb/s DPSK data are simultaneously modulated with a single optical modulator and transmitted over 40-km-long dispersion-shifted fiber (DSF). There exists the received optical power capable of achieving a bit error rate of 10^{-9} simultaneously for both the RF and baseband signals. The degradations due to the nonlinearity of the electroabsorption modulator for the baseband and RF signals are also investigated theoretically and clarified numerically.**

***Index Terms*—Electroabsorption, fiber-to-the-home, millimeter-wave technology, optical fiber communication, radio access networks.**

I. Introduction

FIBER-TO-THE-HOME (FTTH) networks will break the last mile bottleneck in optical access networks, and the demand for broader bandwidth will be further accelerated. There are several options in broad-band use for FTTH systems: one is the large-capacity transmission at baseband, and the other simultaneously uses the baseband and passband in a higher RF carrier. There is an international initiative, the Full Service Access Networks (FSAN), that has set a standard for the access systems supporting a full range of the narrow-band and broad-band services [1]. Recently, this type of scheme has been reported [2]–[5]. In addition, there will be also a growing demand for portable or mobile access, that is, *wireless last hop*, not only to provide broader bandwidth but also to resolve the scarcity of available RF resources; to this end, millimeter-wave technologies are rapidly being developed. The only feasible option to connect the central control station and many microcellular or picocellular antenna base stations in millimeter-wave wireless access systems is the so-called *radio-on-fiber* technique [4]–[6].

Manuscript received January 3, 2001; revised June 20, 2001.

T. Kamisaka and K. Kitayama are with the Department of Electronics and Information Systems, Graduate School of Engineering, Osaka University, Suita, Osaka 565-0871, Japan.

T. Kuri is with the Basic and Advanced Research Division, Communications Research Laboratory (CRL), Koganei, Tokyo 184-8795, Japan (e-mail: kuri@crl.go.jp).

Publisher Item Identifier S 0018-9480(01)08724-5.

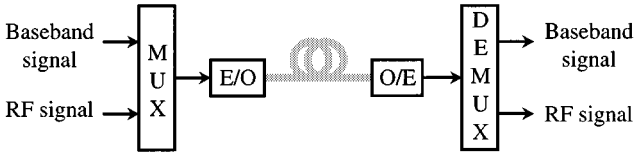

Fig. 1. Fundamental configuration.

In this paper, we will investigate both experimentally and theoretically a simultaneous modulation and fiber-optic transmission of a multigigabit baseband signal and a millimeter-wave-band RF signal on a single wavelength. An electroabsorption modulator (EAM) was adopted as the electrical-to-optical (E/O) converter in a wide range from dc to 60-GHz band [7]. The method is distinct from that in [2] in that it combines digital baseband data and subcarrier signals. It also differs from the method in [3] and [4] in that the two different data signals are transmitted independently at baseband and subcarrier. In addition, unlike the method in [5], our method uses a higher data rate and RF carrier. To the authors' knowledge, it is experimentally demonstrated for the first time that a 10-Gb/s baseband signal and a 60-GHz-band RF signal are simultaneously modulated by a single EAM and transmitted on a single wavelength over a 40-km-long dispersion-shifted fiber (DSF).

II. Simultaneous Modulation and Fiber-Optic Transmission

Fig. 1 shows the conceptual configuration. A sum of a baseband signal, $b(t)$ [$=1$ or -1] and a millimeter-wave-band RF signal with a carrier frequency of $f_{\rm RF}$ and the data of $\theta(t)$ [$=0$ or π] is put into the E/O converter as a modulating signal. This is expressed by $V(t) = A \cdot \cos\{2\pi f_{\rm RF} t + \theta(t)\} + B \cdot b(t)$, where A and B are the amplitudes of the RF and baseband signals, respectively. Here, it is assumed that the RF and baseband signals are separable.

An optical carrier (power: P, frequency: f_c, phase noise: $\phi_{\rm pn}(t)$) is intensity-modulated with $V(t)$. The modulated optical signal after the fiber-optic propagation (length: L) is given as [10]

$$e(t, L) = \sqrt{P} T(V(t)) \cdot \cos\phi(t, L) \tag{1}$$

$$T(V(t)) = \left[(1 + V(t))/2\right]^{\gamma} \tag{2}$$

$$\phi(t, L) = 2\pi f_c t - \beta(f) \cdot L + \phi_{\rm pn}(t) \tag{3}$$

where $\gamma[=(1+j\alpha)/2]$ represents the intensity modulation with the chirp effect (parameter: α). To avoid overmodulation, $|V(t)|$ should be less than 1. Therefore, $A+B \le 1$ is satisfied. The propagation constant $\beta(f)$ is approximately given as $\beta_0 + \beta_1 2\pi(f-f_c) + \beta_2\{2\pi(f-f_c)\}^2/2$ [11]. Here, $\beta_1 L$ corresponds to the group delay time, and $\beta_2 = -\lambda^2 D/2\pi c$ is satisfied, where D, λ, and c are the dispersion and the wavelength in the fiber and the velocity in the vacuum, respectively.

When $|V(t)|$ is small, $e(t, L)$ is approximated as

$$\begin{aligned} e(t,L) \simeq{}& \sqrt{P}\cdot\gamma A\cdot 2^{-\gamma-1}\cdot e^{j\phi_{-1}(t)} \\ &+\sqrt{P}\cdot\{1+\gamma B\cdot b(t)\}\cdot 2^{-\gamma}\cdot e^{j\phi_0(t)} \\ &+\sqrt{P}\cdot\gamma A\cdot 2^{-\gamma-1}\cdot e^{j\phi_1(t)} \end{aligned} \tag{4}$$

$$\begin{aligned} \phi_{-1}(t) \simeq{}& 2\pi f_c t-\beta_0 L+\phi_{\rm pn}(t-\beta_1 L) \\ &-2\pi f_{\rm RF}(t-\beta_1 L)-\theta(t-\beta_1 L) \\ &-(\beta_2/2)\cdot(2\pi f_{\rm RF})^2 L \end{aligned} \tag{5}$$

$$\phi_0(t) \simeq 2\pi f_c t-\beta_0 L+\phi_{\rm pn}(t-\beta_1 L) \tag{6}$$

$$\begin{aligned} \phi_1(t) \simeq{}& 2\pi f_c t-\beta_0 L+\phi_{\rm pn}(t-\beta_1 L) \\ &+2\pi f_{\rm RF}(t-\beta_1 L)+\theta(t-\beta_1 L) \\ &-(\beta_2/2)\cdot(2\pi f_{\rm RF})^2 L. \end{aligned} \tag{7}$$

To concentrate on the serious dispersion effect on the RF signal, the dispersion effect on the baseband signal is neglected. Then, the photocurrent becomes [9]

$$\begin{aligned} I(t,L) &= \left[\mathcal{R}|e(t,L)|^2/2\right]_{\text{at around } f_{\rm RF}} \\ &= (\mathcal{R}P/2)\cdot A\cdot\sqrt{1+(1+\alpha^2)\cdot B^2/4+B\cdot b(t)} \\ &\quad\cdot\sqrt{1+\alpha^2}\cdot\cos\phi_d(t) \\ &\quad\cdot\cos(2\pi f_{\rm RF}(t-\beta_1 L)+\theta(t-\beta_1 L)) \\ &\quad+(\mathcal{R}P/2)\cdot B\cdot b(t) \end{aligned} \tag{8}$$

where $\mathcal{R}$ is the responsivity of the O/E and

$$\begin{aligned} \phi_d(t) = {}& \pi\lambda^2 D L f_{\rm RF}^2/c+\arctan\alpha \\ &+\arctan\left[\{\alpha\cdot B\cdot b(t)\}/\{2+B\cdot b(t)\}\right]. \end{aligned} \tag{9}$$

As the dc and the double-frequency components are not of interest here, they are filtered out. Note that $b^2(t)=1$. It can be seen from (8) and (9) that the baseband data $b(t)$ affect the amplitude of the RF component [the first term of (8)], while nothing affects the baseband data [the second term of (8)].

III. Experiments

A. Setup

Fig. 2 shows the experimental setup. In the transmitter, a baseband signal (9.95328 Gb/s, PRBS $= 2^{23}-1$) is generated from a pulse pattern generator (PPG_1), amplified, and filtered by a low-pass Bessel filter (LPF) with a cutoff frequency of A 60.0-GHz RF signal (155.52-Mb/s, PRBS $= 2^{23}-1$) is also generated with a PPG_2 and a differential-phase-shift-keying (DPSK) modulator. The amplified RF signal is combined with the baseband signal. The optical carrier ($\lambda = 1550.4$ nm) is modulated with a 60-GHz-band EAM [7] by the combined signal. The measured extinction ratio of the EAM used for the

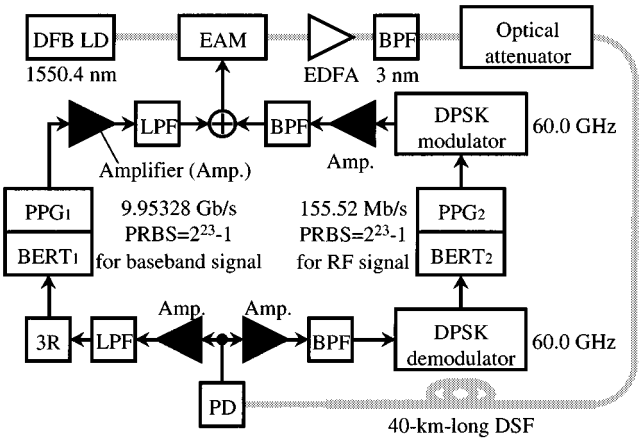

Fig. 2. Experimental setup.

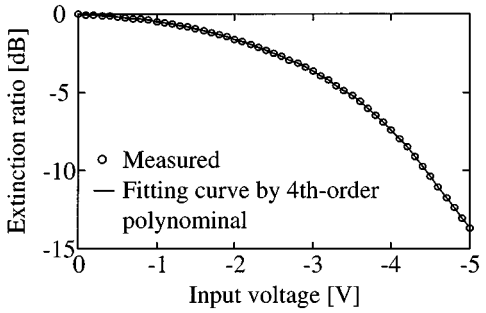

Fig. 3. Extinction ratio of the EAM used.

wavelength of 1550 nm is plotted in Fig. 3. The bias of the EAM was set to -2.7 V, which was optimized to maximize the power of the photodetected RF signal with no baseband signal. The measured chirp parameter α was about 0.75 by using the technique in [9]. The 60-GHz-band return loss (S_{11}) is suppressed in the 3.5-GHz bandwidth because the EAM was designed to optimize at around 60 GHz [7]. As shown in Fig. 4, it was also experimentally confirmed that there exists no serious degradation in the response (S_{21}) from dc to 20 GHz, and an optical link loss of less than 40 dB is achieved. The modulated optical signal is amplified by an erbium-doped fiber amplifier (EDFA). The optical attenuator is inserted to control the transmitting optical power. A 40-km-long DSF ($D = -0.92$ ps/nm/km at 1550.4 nm) was used as a fiber-optic link for the purpose of reducing the fiber dispersion problem as much as possible, instead of using other dispersion compensating techniques [8]. In the remote base station (BS), the received optical signal is detected by a photodetector (PD) and then demodulated separately for the baseband and RF signals. Finally, the bit error rates (BERs) of the baseband and RF signals are measured by BER testers ($BERT_1$ and $BERT_2$), respectively.

B. Results

Fig. 5 shows the measured BERs after the 40-km-long DSF transmission and for the back-to-back transmission. BERs of 10^{-9} for the RF and baseband signals after the DSF transmission were achieved for the received optical powers of -5.7 and -7.4 dBm, respectively. No BER floor was observed for both cases. Surprisingly, the BERs for the back-to-back transmission

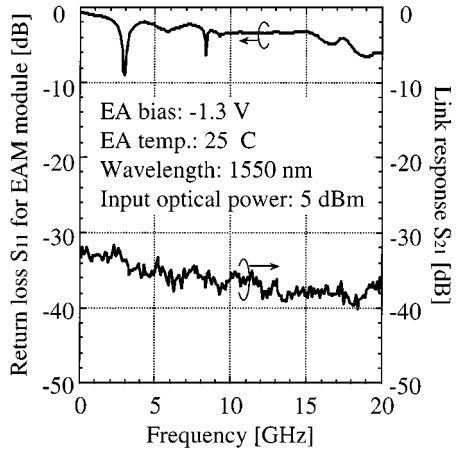

Fig. 4. Measured return loss and its frequency response.

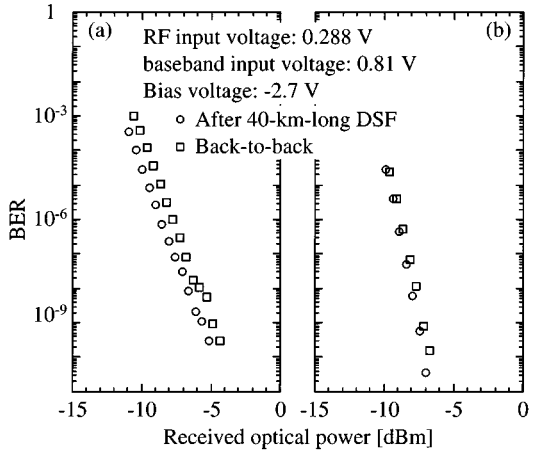

Fig. 5. Measured BERs: (a) for RF signal and (b) for baseband signal.

were worse than that for the DSF transmission. The penalties were about 0.9 and 0.6 dB for the RF and baseband signals, respectively. This is presumably due to the interplay between the chirp of EAM and the fiber group-delay dispersion. It was numerically confirmed that the chirp effect on the baseband and RF signals rather enhance the receiver sensitivities by 1.0 and 0.55 dB, respectively, and those values are very close to the power penalties of the measured BERs.

Fig. 6 shows the received optical powers to achieve a BER of 10^{-9} for the RF and baseband signals. For the RF signal, by increasing the input RF voltage, the required optical power decreases for a constant input baseband voltage. For the baseband signal, the required optical power also decreases for a constant input RF voltage as the input baseband voltage increases. It is also noteworthy that the better BER performance is expected without the counterpart. More details will be discussed in the next section. From Fig. 6, there exists the received optical power capable of achieving a BER of 10^{-9} simultaneously for the RF and baseband signals. As the received optical power becomes larger, the margins of $V_{\rm RF}$ and V_{BB} to simultaneously achieve BERs of 10^{-9} for both baseband and RF signals become wider.

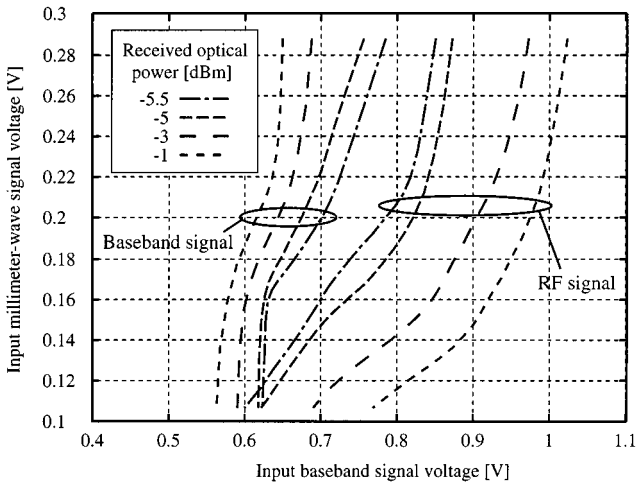

Fig. 6. Received optical power to simultaneously achieve BERs below 10^{-9}.

IV. Discussion—Estimation of Signal Degradation Due to Nonlinearity

Fig. 7 illustrates the distortion affected by the nonlinearity of the EAM. To simplify the theoretical investigation, the chirp of the EAM and the fiber dispersion are neglected ($\alpha = 0$ and $D = 0$). We use the exponential model for the extinction ratio of the EAM

$$T(V) = \exp\left(\sum_{m=0}^{M} g_m V^m\right) = \sum_{n=0}^{\infty} a_n(V_b)\,(V - V_b)^n \tag{10}$$

$$a_n(V_b) = T^{(n)}(V_b)/n!. \tag{11}$$

When $V_{\rm RF}$ [≥ 0] represents the amplitude of the RF signal ($V - V_b = V_{\rm RF}\cos\phi_{\rm RF}(t)$) in voltage and it is small, $T(V)$ is approximately rewritten as

$$T(V) \simeq T_0(V_b) + T_1(V_b)\cdot V_{\rm RF}\cos\phi_{\rm RF}(t) \tag{12}$$

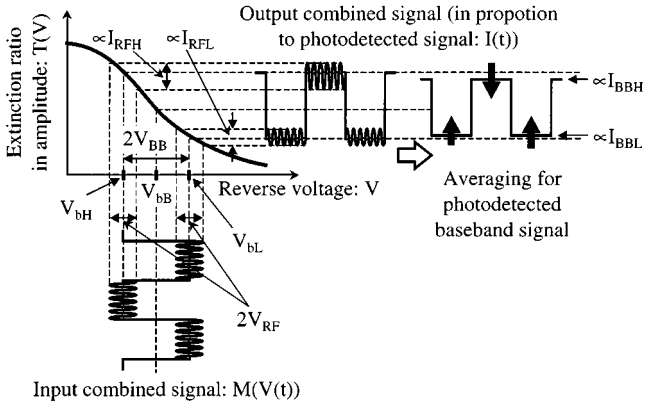

Fig. 7. Nonlinear extinction ratio and distortion to signals.

$$T_0(V_b) = a_0(V_b) + V_{\rm RF}^2\cdot a_2(V_b)/2 + 3V_{\rm RF}^4\cdot a_4(V_b)/8 + \cdots \tag{13}$$

$$T_1(V_b) = a_1(V_b) + 3V_{\rm RF}^2\cdot a_3(V_b)/4 + 5V_{\rm RF}^4\cdot a_5(V_b)/8 + \cdots. \tag{14}$$

Here, $A = |V_{\rm RF}/V_{bB}|$, where V_{bB} is the bias voltage to maximize the photodetected RF power with no baseband signal. From (1) and (12), the photocurrent at around $f_{\rm RF}$ is

$$I(t) = [\mathcal{R}|e(t, L)|^2/2]_{\text{at around } f_{\rm RF}} = \mathcal{R}P \cdot T_0(V_b)T_1(V_b) \cdot V_{\rm RF} \cos\phi_{\rm RF}(t). \quad (15)$$

The bias voltages of the RF signal swings between the high and low levels of the baseband signal, $V_{bH}[=V_{bB}+V_{BB}]$ and $V_{bL}[=V_{bB}-V_{BB}]$, where V_{BB} [$\geq$0] is the amplitude of bipolar baseband signal in voltage and satisfies $B = |V_{BB}/V_{bB}|$. The photocurrent of the baseband at the peak and the bottom are given, respectively, by

$$I_{{\rm RF}H} = \mathcal{R}P \cdot T_0(V_{bH})T_1(V_{bH}) \cdot V_{\rm RF} \quad (16)$$

$$I_{{\rm RF}L} = \mathcal{R}P \cdot T_0(V_{bL})T_1(V_{bL}) \cdot V_{\rm RF}. \quad (17)$$

Taking care of the subcarrier modulation, the average power of the photodetected RF signal becomes $S_{\rm RF} = (I_{{\rm RF}H}^2 + I_{{\rm RF}L}^2) \cdot R_L/4$, where R_L is the load resistance and the equally probable "0"s and "1"s are assumed. To estimate the degradation of RF signal, we introduce the ratio

$$\Delta S_{\rm RF} = S_{\rm RF}/[S_{\rm RF}]_{V_{BB}=0} = \frac{\{T_0(V_{bH})T_1(V_{bH})\}^2 + \{T_0(V_{bL})T_1(V_{bL})\}^2}{2\{T_0(V_{bB})T_1(V_{bB})\}^2}. \quad (18)$$

The reason why $\Delta S_{\rm RF}$ does not depend on $V_{\rm RF}$ is that the linear response for the RF signal is assumed under $A \ll 1$ for simple estimation [see (12)]. We calculated the fitting curve with the measured extinction ratio (Fig. 3) and the fourth-order polynomial in the approximation for (10). g_1, g_2, g_3, and g_4 were 3.14×10^{-2}, -2.50×10^{-2}, -3.04×10^{-4}, and -1.37×10^{-3}, respectively. Fig. 8(a) shows the numerical result of $\Delta S_{\rm RF}$. From the characteristic of exponential function, the slope of the extinction ratio at V_{bH} or V_{bL} is less steep than that at V_{bB}, because V_{bB} is usually set at the point of maximum slope. This is why the power of the photodetected RF signal at V_{bH} or V_{bL} is weaker than that at V_{bB}. In addition, the larger the input amplitude of baseband signal, V_{BB}, becomes, the smaller $\Delta S_{\rm RF}$ gets. This analysis verifies the experimental result in Fig. 6 that by increasing the input baseband voltage the power penalty of RF signal increases for a constant input RF voltage.

The detected levels of the baseband signal will be also degraded by the RF signal, as shown in Fig. 7. In this case, the nonlinear response for the RF signal is considered. By averaging for each level of the baseband signal, the photocurrents for the high and low levels I_{BBH} and I_{BBL} are, respectively,

$$I_{BBH} \simeq (\mathcal{R}P/2) \cdot \{T(V_{bH}+V_{\rm RF}) + T(V_{bH}-V_{\rm RF})\} \quad (19)$$

$$I_{BBL} \simeq (\mathcal{R}P/2) \cdot \{T(V_{bL}+V_{\rm RF}) + T(V_{bL}-V_{\rm RF})\}. \quad (20)$$

The average power of the photodetected baseband signal for the high and low levels, S_{BH} and S_{BL}, are given by $S_{BH} = I_{BBH}^2 \cdot R_L$ and $S_{BL} = I_{BBL}^2 \cdot R_L$, respectively. Fig. 8(b) shows

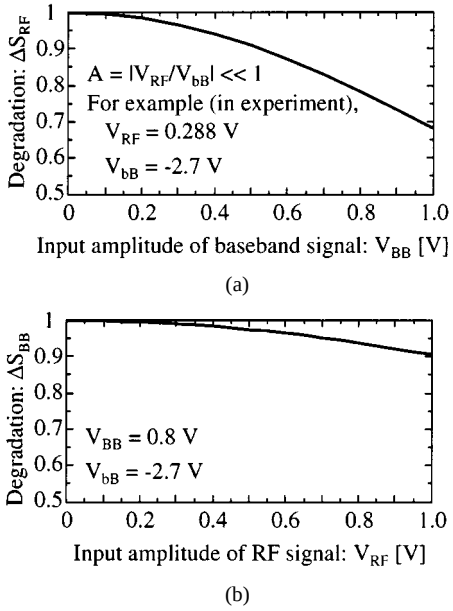

Fig. 8. Degradation for (a) RF and (b) baseband signals.

the numerical result of the degradation for the baseband signal, ΔS_{BB}, which is defined as

$$\Delta S_{BB} = \frac{S_{BH} - S_{BL}}{[S_{BH} - S_{BL}]_{V_{\rm RF}=0}}. \quad (21)$$

I_{BBH} and I_{BBL} are offset from the ideal values, $\mathcal{R}PT(V_{bH})$ and $\mathcal{R}PT(V_{bL})$, due to the RF signal (Fig. 7). The larger the input amplitude of the RF signal, $V_{\rm RF}$, becomes, the smaller ΔS_{BB} becomes. This analysis verifies the experimental result in Fig. 6 that increasing the input RF voltage increases the power penalty of the baseband signal for a constant input baseband voltage.

V. Conclusion

The simultaneous modulation and fiber-optic transmission of both a 9.95328-Gb/s baseband signal and a 155.52-Mb/s-DPSK RF signal at 60 GHz on a single wavelength over a 40-km-long DSF has been investigated both experimentally and theoretically. To the authors' knowledge, this was the first investigation of the simultaneous transmission with the 60-GHz-band EAM module that achieved BERs of less than 10^{-9} simultaneously for the baseband and RF signals. The performance degradations due to the undesired nonlinearity of the EAM have also been investigated theoretically and clarified numerically. As a result, the numerical tendencies agreed with the experimental results.

This technique will serve to effectively provide wide bandwidths both with FTTH and wireless access systems in the future.

Acknowledgment

The authors wish to thank Y. Tomiyama, Communications Research Laboratory (CRL), Tokyo, Japan, and T. Kawanishi, CRL, Tokyo, Japan, and T. Ushikubo, Oki Electric Industry Company Ltd. for their collaboration. One of the authors, T. Kuri, also wishes to thank N. Otani, CRL, Tokyo, Japan, W.

Chujo, CRL, Tokyo, Japan, K. Itabe, CRL, Tokyo, Japan, and T. Iida, CRL, Tokyo, Japan, for their encouragement.

REFERENCES

[1] Full Service Access Networks (FSAN), Gx Initiative Documents Collection on World Wide Web. [Online]; also ITU Document G.983. Available: http://www.fsanet.net

[2] N. Cand, P. Magill, V. Swaminathan, and T. H. Daugherty, "Delivery of >1 Gb/s (digital video, data, and audio) downstream in passband above the 155-Mb/s baseband services on a FTTx full service access network," *IEEE Photon. Technol. Lett.*, vol. 11, pp. 1192–1194, Sept. 1999.

[3] V. Polo, A. Martinez, J. Marti, F. Ramos, A. Griol, and R. Llorente, "Simultaneous baseband and RF modulations scheme in Gbit/s millimeter-wave wireless-fiber networks," in *Int. Microwave Photon. Top. Meeting Tech. Dig.*, Oxford, U.K., 2000, WE2.5, pp. 168–171.

[4] C. Lim, A. Nirmalathas, D. Novak, R. Waterhouse, and K. Ghorbani, "Full-duplex broadband fiber-wireless system incorporating baseband data transmission and a novel dispersion tolerant modulation scheme," in *Proc. Int. Microwave Symp.*, vol. 3, 1999, WE4B-1, pp. 1201–1204.

[5] D. J. Blumenthal, J. Laskar, R. Gaudino, S. Han, M. D. Schell, and M. D. Vaughn, "Fiber-optic links supporting baseband data and subcarrier-multiplexed control channels and the impact of MMIC photonic/microwave interfaces," *IEEE Trans. Microwave Theory Tech.*, vol. 45, pp. 1443–1452, Aug. 1997.

[6] T. Kuri, K. Kitayama, and Y. Ogawa, "Fiber-optic millimeter-wave uplink system incorporating remotely fed 60-GHz-band optical pilot tone," *IEEE Trans. Microwave Theory Tech.*, vol. 47, pp. 1332–1357, July 1999.

[7] T. Kuri, K. Kitayama, A. Stöhr, and Y. Ogawa, "Fiber-optic millimeter-wave downlink system using 60-GHz-band external modulation," *J. Lightwave Technol.*, vol. 17, pp. 799–806, May 1999.

[8] For example and K. Kitayama, "Ultimate performance of optical DSB signal-based millimeter-wave fiber-radio system: Effect of laser phase noise," *J. Lightwave Technol.*, vol. 17, pp. 1774–1781, Oct. 1999.

[9] F. Devaux, Y. Sorel, and J. K. Kerdiles, "Simple measurement of fiber dispersion and of chirp parameter of intensity modulated light emitter," *J. Lightwave Technol.*, vol. 11, pp. 1937–1940, Dec. 1993.

[10] M. Suzuki, Y. Noda, and Y. Kushiro, "Characterization of a dynamic spectral width of an InGaAsP/InP electroabsorption light modulator," *Trans. IEICE*, vol. E69, no. 4, pp. 395–398, Apr. 1986.

[11] G. P. Agrawal, *Nonlinear Optics*, 2nd ed: Academic, 1995, Secs. 2–4.

[12] R. B. Welstand, J. T. Zhu, W. X. Chen, A. R. Clawson, P. K. L. Yu, and S. A. Pappert, "Combined Franz–Keldysh and quantum-confined Stark effect waveguide modulator for analog signal transmission," *J. Lightwave Technol.*, vol. 17, pp. 497–502, Mar. 1999.

Tomotada Kamisaka received the B.E. degree from National Institution for Academic Degrees, Yokohama, Japan, in 1999 and the M.E. degree from Osaka University, Osaka, Japan, in 2001.

He is currently an Electric Technical Expert.

Mr. Kamisaka is a member of the Institute of Electronics, Information and Communication Engineers (IEICE), Japan.

Toshiaki Kuri (S'93–M'96) received the B.E., M.E., and Ph.D. degrees from Osaka University, Osaka, Japan, in 1992, 1994, and 1996, respectively.

In 1996, he joined Communications Research Laboratory, Ministry of Posts and Telecommunications, Tokyo, Japan, where he is mainly engaged in the research on optical communication systems.

Dr. Kuri is a member of the Institute of Electronics, Information and Communication Engineers (IEICE), Japan. He was the recipient of the 1998 Young Engineer Award from the IEICE.

Ken-ichi Kitayama (S'75–M'76–SM'89) received the B.E., M.E., and Dr. Eng. degrees in communication engineering from Osaka University, Osaka, Japan, in 1974, 1976, and 1981, respectively.

In 1976, he joined the NTT Electrical Communication Laboratory. From 1982 to 1983, he spent a year as a Research Fellow at the University of California at Berkeley. In 1995, he joined the Communications Research Laboratory, Tokyo, Japan. Since 1999, he has been with Osaka University, where he is currently the Professor of the Department of Electronic and Information Systems Engineering, Graduate School of Engineering. His research interests include photonic networks and fiber-optic wireless communications. He has authored or co-authored over 140 papers in refereed journals, two book chapters, and translated one book. He holds over 30 patents.

Prof. Kitayama is a member of the the Institute of Electronic, Information and Communication Engineers (IEICE), Japan, the Japan Society of Applied Physics, and the Optical Society of Japan. He currently serves on the Editorial Boards of the IEEE PHOTONICS TECHNOLOGY LETTERS and the IEEE TRANSACTIONS ON COMMUNICATIONS. He was the recipient of the 1980 IEICE Young Engineer Award f and the 1985 Paper Award of Optics presented by the Japan Society of Applied Physics.